ICP **Imperial College Press**
www.icpress.co.uk

PRESSURE DRIVEN STEADY FLOW IN CONSTRICTED CHANNELS OF DIFFERENT CROSS-SECTION SHAPES

B. WU and A. VAN HIRTUM*

GIPSA-Lab, UMR CNRS 5216
Grenoble University, France
!annemie.vanhirtum@gipsa-lab.grenoble-inp.fr

X. Y. LUO

School of Mathematics and Statistics
University of Glasgow, Glasgow G12 8QW, UK

The influence of the cross-section shape on pressure driven viscous flow through a uniform channel is assessed by presenting analytical flow solutions of velocity distribution, volume flow rate and shear stress for different cross-section shapes. Next, a simplified flow model through a non-uniform constricted channel is formulated which accounts for flow inertia, viscosity and cross-section shape. The model outcome is quantified for different fluids, flows and geometrical properties relevant to physiological flows. It is seen that a commonly applied quasi-one-dimensional (1D) model is not accurate indicating the need to account for the cross-section shape.

Keywords: Laminar viscous flow; analytical flow model; respiratory flow; stenosis.

1. Introduction

Pressure driven channel flow is associated with physiological flows for which constricted channel portions occur either naturally or due to a pathology. Well-known examples are airflow through the human airways (human speech production, asthma, obstructive sleep apnea) or blood flow through a stenosis.

Consequently, efforts are made to model pressure driven flow through constricted channels in order to understand the mechanisms involved and to develop aiding tools for healthcare workers such as surgeons, medical doctors, speech therapists, prosthesis designers (dental or glottal), aerosol spray designers, etc. Due to the complexity of the human respiratory and cardiovascular system, most studies severely simplify the physiological reality in order to come up with a configuration depending on a limited number of meaningful physiological and physical parameters [Lucero *et al.*, 2000]. Such a simplification enhances understanding of the ongoing physical

phenomena and facilitates experimental validation of the models accuracy [Shapiro, 1977; Pedley and Luo, 1998; Cisonni *et al.*, 2008; Lorthois *et al.*, 2009 and Stewart *et al.*, 2010].

In general, simplifications of the flow model through portions of the respiratory or cardiovasculars system are based on a non-dimensional analysis of the governing Navier–Stokes equations [Batchelor, 2000]. Accounting for typical values of physiological, geometrical and flow characteristics result in non-dimensional numbers (Mach number, Reynolds number, Strouhal number and mean aspect ratio) which allows one to assume the flow as incompressible, laminar, quasi-1D or 2D and quasi-steady. As an example typical Reynolds numbers Re are Re $< 10^3$ for blood flow and Re $< 10^4$ for respiratory airflow. Therefore, quasi-1D or 2D flow models derived from the boundary layer theory have proven to be extremely useful to capture the underlying physics and are applied to mimic and predict ongoing phenomena using few computational resources while allowing experimental validation on replicas with a different degree of complexity [Van Hirtum *et al.*, 2009; Cisonni *et al.*, 2010; Chouly and Lagrée, 2012].

Nevertheless, the assumption of a 1D or 2D geometry implies that details of the cross-section shape perpendicular to the streamwise flow direction x are neglected. Viscous effects, which will dominate flow development at low Reynolds numbers, are known to depend on the cross-section shape [Batchelor, 2000]. The aim of the present paper is, therefore, to propose a flow model capable to account for flow inertia, viscosity as well as for the cross-section shape.

In the following, assessed cross-section shapes are described in Sec. 2. The influence of the cross-section shape on pressure driven viscous flow through uniform channels with different cross-section shapes is assessed analytically in Sec. 3.1. Next, a simplified flow model is presented accounting for flow through a constricted channel with different cross-section shape (Sec. 3.2). Finally, model results are presented and discussed in Sec. 4.

2. Channel Cross-Section Shapes

The channel geometry is fully defined by the cross-section shape and area variation along the streamwise flow direction x. In order to use the cross-section shape in quasi-analytical models, only shapes for which the geometry can be expressed analytically using one or two geometrical parameters are assessed: circle (cl), rectangle (re), ellipse (el), eccentric annulus (ea), concentric annulus (ca), half-moon (hm), circular segment (cs), equilateral triangle (tr) and limacon (lm). Different cross-section shapes and associated geometrical parameters are illustrated in Fig. 1 with y denoting the spanwise and z the transverse direction.

The chosen shapes have, although a severe idealization, some relevance to describe the channel cross-section shape in the case of normal as well as pathological geometrical conditions of the human respiratory and cardiovascular systems. The circular, rectangular and elliptical cross-section shapes are idealized shapes
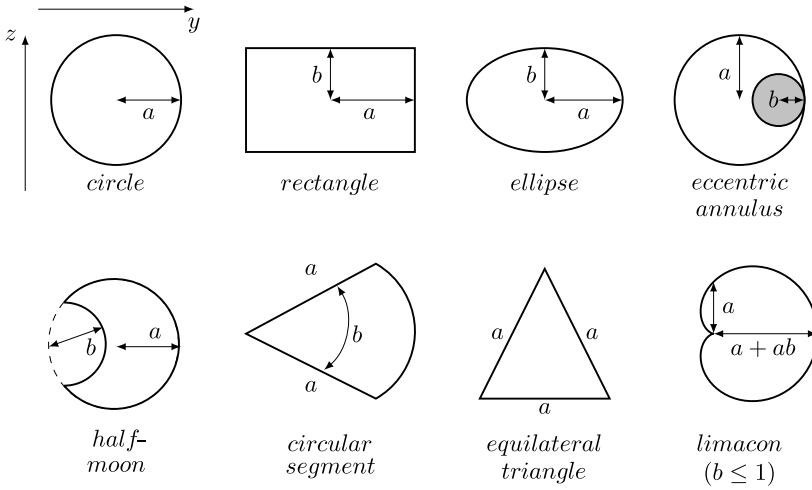
Fig. 1. Cross-section shapes with parameters (a, b) in the (y, z) plane. Note that for a circular segment, b indicates an angle.

assuming a perfect symmetry of the channel or the constricted portion with respect to the spanwise y and transverse z directions. The eccentric annulus, half-moon and limacon are crude approximations to an asymmetrical shape due to e.g., the presence of a polyp, a tumor, an asymmetrical stenosis or a vocal tract articulator. The circular segment and the equilateral triangle are approximations of asymmetrical cross-section shapes occurring e.g., at the glottis during normal respiration. Comparison between different geometries is made by imposing either area A or hydraulic diameter D. Cross-section shapes which are defined using two instead of one geometrical parameter require an additional condition. Expressions for A, D and total width y_{tot} as function of geometrical parameters (a, b) are given in Appendix A.

3. Analytical Flow Model

The flow model and underlying assumptions for pressure driven flow through a uniform and constricted channel portion is outlined in Secs. 3.1 and 3.2, respectively. Within the context of physiological fluids both air and blood are considered for which characteristic fluid properties are summarized in Table 1.

Table 1. Overview fluid properties.

	Dynamic viscosity, μ [Pa.s]	Density, ρ [kg/m^3]
Blood	3.5×10^{-3}	1060
Air	1.8×10^{-5}	1.2
Ratio[a]	194	883

[a]Ratio of blood property to air property.

3.1. *Viscous flow: Cross-section shape*

For a given fluid with dynamic viscosity μ and under the assumptions of laminar, incompressible, parallel and steady viscous flow through a uniform channel with arbitrary but constant cross-section shape, the streamwise component of the momentum equation expressed in Cartesian coordinates (x, y, z) reduces to the following Poisson equation [White, 1991; Batchelor, 2000]:

$$\frac{1}{\rho}\frac{dP}{dx} = \nu\left(\frac{\partial^2 u}{\partial y^2} + \frac{\partial^2 u}{\partial z^2}\right),\tag{1}$$

with driving pressure gradient dP/dx, velocity $u(y, z)$ and kinematic viscosity $\nu = \mu/\rho$. The spanwise and transverse components of the momentum equation become:

$$\frac{\partial P}{\partial y} = 0, \quad \frac{\partial P}{\partial z} = 0\tag{2}$$

and the continuity equation yields:

$$\frac{\partial u}{\partial x} = 0.\tag{3}$$

For uniform geometries and applying the no-slip boundary condition $u = 0$ on the channel walls, Eq. (1) can be rewritten as a classical Dirichlet problem which can be solved analytically for simple geometries using e.g., separation of variables or conformal mapping [Berker, 1963; Shah and London, 1978; Milne-Thomson, 1996; Gutmark and Grinstein, 1999; Lekner, 2007]. Therefore exact solutions can be obtained for: local velocity $u(y, z)$, local pressure $P(x)$, wall shear stress $\tau(x)$ and derived quantities such as volume flow rate Q. In the following analytical solutions are given of which some are validated by expressions reported in literature [Papanastasiou *et al.*, 2000; White, 1991; Macdonald, 1893; Piercy *et al.*, 1933; Haslam and Zamir, 1998; Berker, 1963].

Analytical solutions for the volume flow rate can be generally described by an expression of the form

$$Q = \beta_q(a, b)\frac{1}{\mu}\left(-\frac{dp}{dx}\right),\tag{4}$$

for which β_q, given in Table 2, depends on the cross-section shape and its parameters (a, b). It is seen that for all cross-section shapes the resulting volume flow rate is proportional to the ratio of the driving pressure gradient dP/dx to the dynamic viscosity μ. Expression (4) also holds in the case of a quasi-1D flow model approach [Cisonni *et al.*, 2008] for which the viscous contribution to the pressure drop is accounted for by a Poiseuille term assuming a rectangular cross-section with fixed width w and height h.

It is easily seen that besides the volume flow rate, Q is also the velocity distribution, $u(y, z)$ is proportional to the ratio of the driving pressure gradient dP/dx

Table 2. $\beta_q(a, b)$ of Eq. (4) for volume flow rate Q [Papanastasiou *et al.*, 2000; White, 1991; Piercy *et al.*, 1933; Berker, 1963].

Shape	$\beta_q(a, b)$
Circle	$\dfrac{\pi a^4}{8}$
Ellipse	$\dfrac{\pi}{4} \dfrac{a^3 b^3}{a^2 + b^2}$
Rectangle[a]	$\dfrac{4a^3}{3} \left[b - \dfrac{192a}{\pi^5} \displaystyle\sum_{n=1,3,\dots}^{\infty} \dfrac{\tanh(n\pi b/2a)}{n^5} \right]$
Equilateral triangle	$\dfrac{\sqrt{3}a^4}{320}$
Circular segment[a]	$\dfrac{a^4}{4} \left[\dfrac{\tan b - b}{4} - \dfrac{32b^4}{\pi^5} \displaystyle\sum_{n=1,3\dots}^{\infty} \dfrac{1}{n^2(n + 2b/\pi)^2(n - 2b/\pi)} \right]$
Eccentric annulus[a,b]	$\dfrac{\pi}{8} \left[a^4 - b^4 - \dfrac{4c^2 M^2}{\beta - \gamma} - 8c^2 M^2 \displaystyle\sum_{n=1}^{\infty} \dfrac{ne^{-n(\beta+\gamma)}}{\sinh(n\beta - n\gamma)} \right]$
	$0 < c \le a - b, \ F = \dfrac{a^2 - b^2 + c^2}{2c}$
	$M = \sqrt{F^2 - a^2}$
	$\gamma = \dfrac{1}{2} \ln \dfrac{F + M}{F - M}, \ \beta = \dfrac{1}{2} \ln \dfrac{F - c + M}{F - c - M}$
Concentric annulus	$\dfrac{\pi}{8} \left[a^4 - b^4 - \dfrac{(a^2 - b^2)^2}{\ln \dfrac{a}{b}} \right]$
Half-moon	$\dfrac{1}{4} \left[\left(2a^3 b + \dfrac{21}{12} ab^3 \right) \sin(\theta_1) + \left(a^4 - \dfrac{b^4}{2} - 2a^2 b^2 \right) \theta_1 \right]$
	$\theta_1 = \arccos(b/2a)$
Limacon	$\dfrac{\pi}{8} a^4 \left(1 + 4b^2 - 2b^4 \right)$
Poiseuille[c]	$\dfrac{wh^3}{12}$

[a]Infinite sum is limited to $n \le 60$.
[b]c yields the distance between inner and outer circle centers.
[c]Quasi-1D approach: height h and fixed width w.

and the dynamic viscosity μ so that the following holds using Eq. (4):

$$u = \beta_u(a, b) \frac{1}{\mu} \left(-\frac{dp}{dx} \right) \quad \text{or} \quad u = Q \frac{\beta_u(a, b)}{\beta_q(a, b)}, \tag{5}$$

in which $\beta_u(a, b)$ gathers the influence of the cross-section shape on the velocity distribution.

The wall shear stress,

$$\tau = \beta_t(a, b) \left(\frac{dp}{dx} \right), \tag{6}$$

depends on the driving pressure gradient dP/dx and the cross-section shape $\beta_t(a,b)$. Expressions $\beta_u(a,b)$ for the associated velocity distribution and $\beta_t(a,b)$ for the associated wall shear stress τ are given in Appendix B.

From expression (4), it follows that the viscous contribution to the pressure drop is:

$$\Delta P_{\text{visc}}(x) = -\mu Q \int_{x_0}^{x} \frac{dx}{\beta_q(a,b)}, \tag{7}$$

with x_0 denoting the channel onset and $x > x_0$. Consequently, ΔP_{visc} varies linearly with volume flow rate Q and dynamic viscosity μ and is inversed proportional to the cross-section shape factor β_q.

3.2. *Flow acceleration: Varying streamwise area*

For pressure driven flow through a channel with varying streamwise area $A(x)$ involving a constricted portion, flow inertia cannot be neglected [White, 1991; Batchelor, 2000]. Therefore, the streamwise component of the momentum equation is approximated as:

$$-\frac{Q^2}{A^3}\frac{dA}{dx} + \frac{1}{\rho}\frac{dP}{dx} = \nu\left(\frac{\partial^2 u}{\partial y^2} + \frac{\partial^2 u}{\partial z^2}\right), \tag{8}$$

using $dQ/dx = 0$, whereas the spanwise and transverse components of the momentum equation are described by (2). It is easily seen that for a uniform channel $dA/dx = 0$ holds so that (8) reduces to purely viscous flow described by (1). Neglecting viscosity, i.e., $\nu = 0$, is seen to reduce (8) to the inviscid Euler equation for which the contribution to the pressure drop is:

$$\Delta P_{\text{ber}}(x) = \frac{\rho}{2}Q^2\left(\frac{1}{A(x)^2} - \frac{1}{A_0^2}\right), \tag{9}$$

with A_0 denoting the unconstricted channel area at the inlet.

The right-hand side of (8) still contains the spanwise and transverse component and adds therefore a 3D aspect to the model. Classical simplified flow models either make a 2D assumption by neglecting the spanwise dimension [Van Hirtum *et al.*, 2009; Cisonni *et al.*, 2010; Chouly and Lagrée, 2012] or fully reduce the problem to a 1D model for which the right-hand side of (8) is reduced to a flow resistance term characterized by a constant [Shapiro, 1977; Pedley and Luo, 1998; Stewart *et al.*, 2010].

In the following, a constricted channel with a smooth or an abrupt diverging area portion is accounted for, as depicted in Fig. 2. For an abrupt expansion characterized by a sharp trailing edge, the streamwise position of flow separation x_s is fixed and coincides with the trailing end of the constriction, so that $x_s = x_3$ as depicted in Fig. 2(b). In the case of a smooth expansion, the flow separation position depends on the channel geometry as well as on the imposed driving pressure gradient dP/dx,
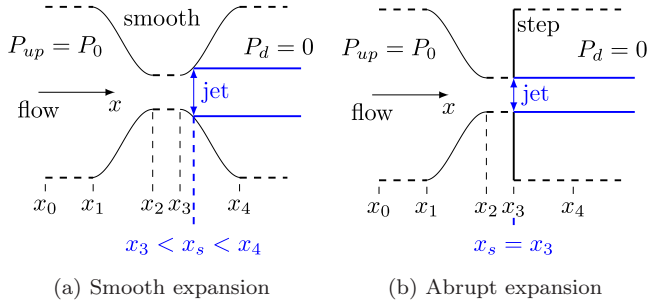
(a) Smooth expansion   (b) Abrupt expansion

Fig. 2. Flow within a converging diverging geometry with upstream area A_0 and minimum area $A_{\min}$ for (a) a smooth and (b) an abrupt expansion.

so that $x_3 \leq x_s \leq x_4$ as illustrated in Fig. 2(a) and the position of flow separation needs to be determined.

The separation position $x = x_s$ corresponds to the position along the diverging portion where the area yields $A(x_s) = c_s \times A_{\min}$ with $c_s = 1.2$. This *ad hoc* criterion is commonly used and validated for a quasi-1D flow model approach [Van Hirtum *et al.*, 2009; Cisonni *et al*, 2010; Lucero *et al.*, 2009]. The pressure downstream from the flow separation point is assumed to be zero so that $P_d = 0$ holds for $x \geq x_s$ and the model outcome remains constant for $x \geq x_s$. Consequently, imposing the upstream pressure $P_{up} = P_0$ yields a total driving pressure gradient $dP/dx = P_0$.

Therefore, the same way as for a quasi-1D flow model [Cisonni *et al.*, 2008; Van Hirtum *et al.*, 2009], firstly, the volume flow rate Q can be estimated from the imposed pressure gradient using (8). Next, the streamwise distribution of other quantities such as the pressure distribution up to flow separation can be derived since from (8), it is easily seen that,

$$P_{up} - P_d = \Delta P_{visc} + \Delta P_{ber}, \tag{10}$$

holds with ΔP_{visc} and ΔP_{ber} as defined in (7) and (9).

4. Results

In the following, the influence of the cross-section shape on the model outcome is assessed for a uniform channel (Sec. 4.1) and for a varying converging diverging area (Sec. 4.2).

The comparison between different cross-section shapes is assessed by imposing either area A or hydraulic diameter D. As mentioned in Sec. 2, the circle and equilateral triangle cross-section shapes are fully described by one parameter, a_{cl} and a_{tr}, whose value follows immediately from the imposed A or D. For the remaining cross-section shapes, an additional condition is necessary in order to obtain the geometrical parameter set $\{a, b\}$ illustrated in Fig. 1. Two different types of additional conditions are considered. Firstly, an explicit condition requiring a parameter α_{shape} is introduced scaling the cross-section shape as: $a_{re} = \alpha_{re}a_{cl}$, $a_{el} = \alpha_{el}a_{cl}$,
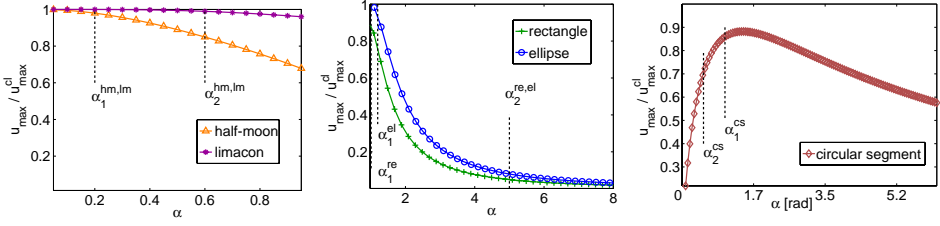
Fig. 3. Illustration of the influence of geometrical parameter α on normalized maximum velocity, $u_{\max}/u_{\max}^{\mathrm{cl}}$, for different cross-section shapes and imposed area $A = 79\,\mathrm{mm}^2$. Vertical lines indicate values corresponding to parameter set 1 (α_1) and parameter set 2 (α_2) for which $u_{\max}/u_{\max}^{\mathrm{cl}} \approx 1$ and $u_{\max}/u_{\max}^{\mathrm{cl}} \ll 1$, respectively.

$b_{\mathrm{ea}} = \alpha_{\mathrm{ea}} a_{\mathrm{ea}}$, $b_{\mathrm{cs}} = \alpha_{\mathrm{cs}}$, $b_{\mathrm{hm}} = \alpha_{\mathrm{hm}} a_{\mathrm{hm}}$ and $b_{\mathrm{lm}} = \alpha_{\mathrm{lm}}$. Secondly, the required additional condition is obtained by imposing, besides area A or hydraulic diameter D, a fixed width w.

4.1. *Velocity distribution: Uniform channel*

The ratio of maximum velocity $u_{\max}$ and maximum velocity for a circular cross-section shape $u_{\max}^{\mathrm{cl}}$ is assessed for an imposed area $A = 79\,\mathrm{mm}^2$ in order to estimate the influence of the cross-section shape. The ratio $u_{\max}/u_{\max}^{\mathrm{cl}}$ is constant for a circle ($= 1$) and equilateral triangle ($= 0.8$) since their shapes do not depend on the parameter α. For all other cross-section shapes, the choice of the parameter α does influence to some extent the velocity distribution as shown in Fig. 3 by considering the deviation of $u_{\max}/u_{\max}^{\mathrm{cl}}$ from 1.

It is seen that varying the cross-section shape by increasing α from 0 (corresponding to a circle) to 0.95 reduces the maximum velocity within 40% for a half-moon and within 5% for a limacon cross-section shape. Varying the cross-section shape by increasing α from $\sqrt{\pi/4}$ (corresponding to a square) for a rectangular and from 1 (corresponding to a circle) for an ellipse to 8 reduces the maximum velocity with 97%. For a circular segment, increasing the angle α from $0°$, at first increases the maximum velocity until $\alpha_{\mathrm{cs}} \simeq 85°$. Further increasing the angle causes the maximum velocity to decrease again. Consequently, Fig. 3 shows that for a constant area A and cross-section shape, the scaling parameter α influences the effect of viscosity on the flow development since the variation of the ratio $u_{\max}/u_{\max}^{\mathrm{cl}}$ with α is significant for all cross-section shapes.

In order to evaluate the impact of the cross-section shape in more detail, two sets of parameters α are selected, parameter set 1 (α_1) and parameter set 2 (α_2), resulting in $u_{\max}/u_{\max}^{\mathrm{cl}} \approx 1$ and $u_{\max}/u_{\max}^{\mathrm{cl}} \ll 1$, respectively. Parameter set 1 (α_1) is defined as: $a_{\mathrm{re}} = 1a_{\mathrm{cl}}$, $a_{\mathrm{el}} = 1.2a_{\mathrm{cl}}$, $b_{\mathrm{ea}} = 0.2a_{\mathrm{ea}}$, $b_{\mathrm{cs}} = \pi/3$, $b_{\mathrm{hm}} = 0.2a_{\mathrm{hm}}$ and $b_{\mathrm{lm}} = 0.2$. Parameter set 2 (α_2) yields: $a_{\mathrm{re}} = 5a_{\mathrm{cl}}$, $a_{\mathrm{el}} = 5a_{\mathrm{cl}}$, $b_{\mathrm{ea}} = 0.6a_{\mathrm{ea}}$, $b_{\mathrm{cs}} = \pi/6$, $b_{\mathrm{hm}} = 0.6a_{\mathrm{hm}}$ and $b_{\mathrm{lm}} = 0.6$. Both parameter sets are indicated in Fig. 3.

Three different cross-section shapes are obtained by imposing area A together with parameter set 1 (α_1), parameter set 2 (α_2) or fixed width w. The resulting
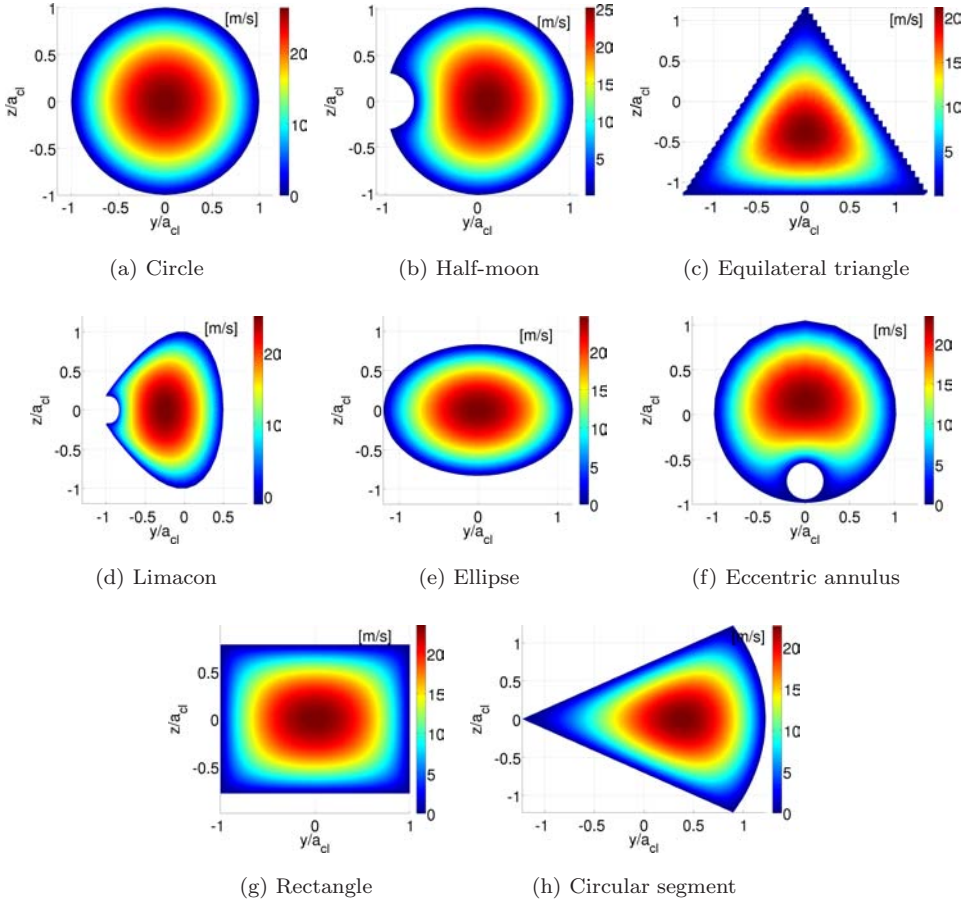
Fig. 4. Velocity distribution $u(y/a_{cl}, z/a_{cl})$ for $A = 79\,\mathrm{mm}^2$ and $dP/dx = 75$ Pa for airflow and geometrical parameter set 1 (α_1).

velocity distribution $u(y/a_{cl}, z/a_{cl})$ for a uniform channel with imposed area $A = 79\,\mathrm{mm}^2$ and pressure gradient $dP/dx = 75$ Pa is illustrated in Fig. 4 for parameter set 1 (α_1) and in Fig. 5 for parameter set 2 (α_2) and fixed width, (w).

From Fig. 4, obtained by using parameter set 1 (α_1), it is seen that in accordance with Fig. 3 the maximum velocity for all cross-section shapes varies between values observed for a circular and an equilateral triangle cross-section shape so that the maximum velocity reduction compared to a circular cross-section yields 20%. From Fig. 5 it is seen that using parameter set 2 (α_2) or imposing a fixed width (w) reduces the velocity more (20% up to 98%).

The influence of the cross-section shape on the maximum velocity is further quantified in Fig. 6 by imposing either area $A = 79\,\mathrm{mm}^2$ or the corresponding hydraulic diameter $D = 10\,\mathrm{mm}$ in combination with parameter set 1 (α_1), parameter set 2 (α_2) or fixed width (w).

(a) Ellipse (b) Eccentric annulus (c) Half-moon

(d) Circular segment (e) Ellipse (f) Eccentric annulus
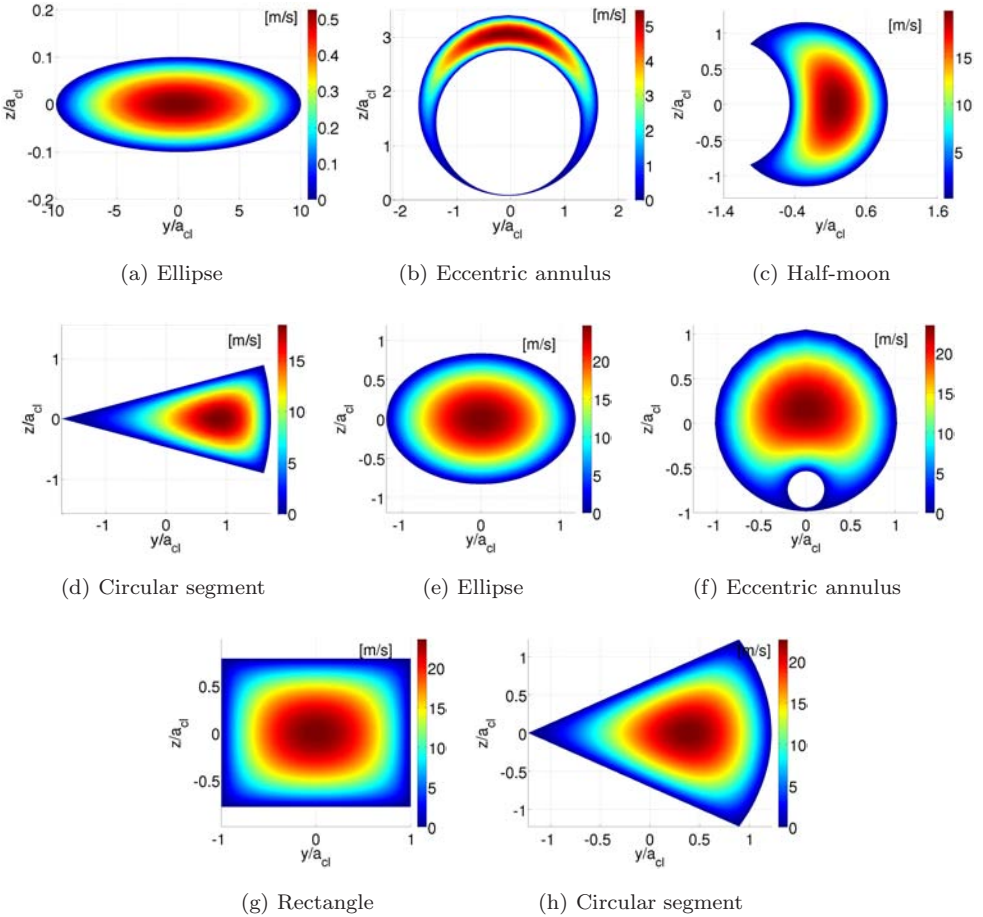
(g) Rectangle (h) Circular segment

Fig. 5. Velocity distribution $u(y/a_{cl}, z/a_{cl})$ for $A = 79\,\text{mm}^2$ and $dP/dx = 75$ Pa for airflow: (a)–(d) geometrical parameter set 2 (α_2) and (e)–(h) fixed width (w) with $w = 4 \times a_{cl}$.

Figure 6(a) shows the maximum velocity normalized with respect to the maximum velocity of a rectangular cross-section shape. As before, the variation from $u_{\text{max}}^{\text{re}}$ for parameter set 1 (α_1) is small, yielding less than 5% when imposing A and less than 15% when imposing D. For fixed area A, the variation from $u_{\text{max}}^{\text{re}}$ increases to 60% in the case of a fixed width w and to more than 300% when parameter set 2 (α_2) is used. Imposing the hydraulic diameter D instead of area A limits the velocity variation to 60% for both parameter set 2 (α_2) and fixed width w.

Figure 6(b) illustrates for each cross-section shape the ratio of the maximum velocity of parameter set 1 (α_1) to the maximum velocity obtained using parameter set 2 (α_2) or a fixed width (w). The relative difference between different parameter sets is limited to 40% when the hydraulic diameter D is imposed. In the case where area A is imposed, the velocity ratio varies from 40% up to $>100\%$.

(a) Cfr. rectangular cross-section
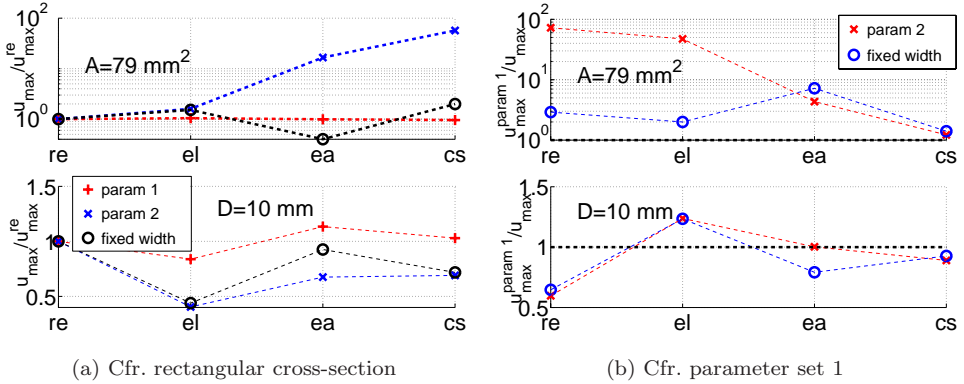
(b) Cfr. parameter set 1

Fig. 6.   Illustration of influence of cross-section shapes (re: rectangular, el: ellipse, ea: eccentric annulus, cs: circular segment) obtained from imposing different conditions (parameter set 1 (α_1), parameter set 2 (α_2) and fixed width (w)) for imposed area $A = 79\,\mathrm{mm}^2$ or hydraulic diameter $D = 10\,\mathrm{mm}$ on the maximum velocity: (a) with respect to maximum velocities associated with a rectangular cross-section and (b) with respect to maximum velocities associated with parameter set 1. The dashed line corresponds to $u_{\max}^{\mathrm{param1}}/u_{\max} = 1$.
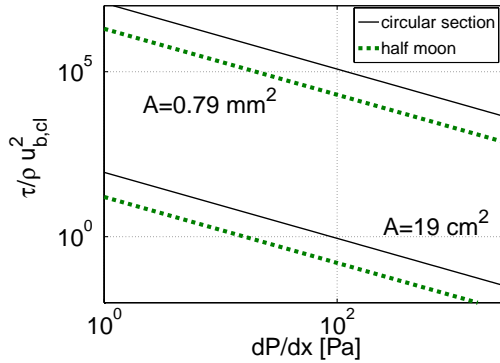

Fig. 7.   Normalized wall shear stress $\tau(dP/dx, A)$.

The mean wall shear stress on the boundary of the cross-section shape as function of driving pressure gradient dP/dx is illustrated in Fig. 7. The wall shear stress increases as driving pressure gradient dP/dx decreases or as area A decreases.

4.2. *Pressure distribution: Varying streamwise area*

The pressure distribution in a constricted channel with varying streamwise area for different cross-section shapes is assessed using parameter set 1 (α_1), parameter set 2 (α_2) and fixed width, (w), defined in Sec. 4.1, for different flow, fluid and geometrical configurations.

Figure 8 illustrates the pressure distribution for a smooth and abrupt expansion when the area $A = 79\,\mathrm{mm}^2$ is imposed using parameter set 1 and $P_0 = 75$ Pa. In

(a) Parameter set 1, smooth expansion

(b) Parameter set 1, abrupt expansion
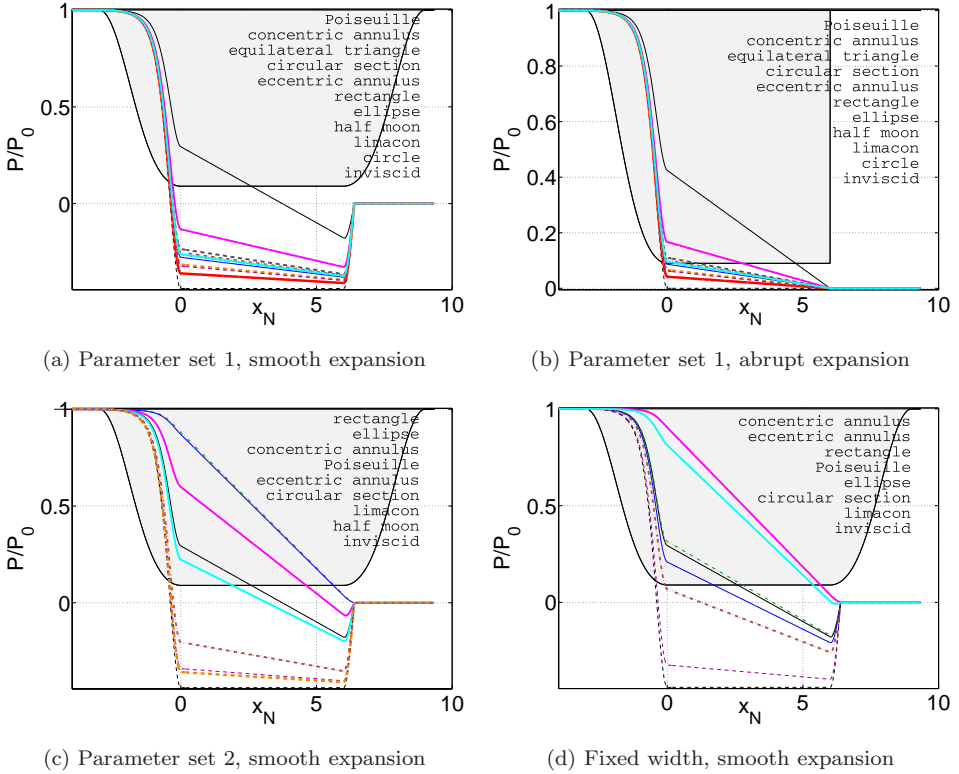
(c) Parameter set 2, smooth expansion

(d) Fixed width, smooth expansion

Fig. 8. Illustration of pressure distribution for airflow and imposing area $A = 79$ mm^2, $P_0 = 75$ Pa, $R_c = 30\%$ and $L_c = 6$ for different cross-section shapes obtained using (a), (b) parameter set 1, (c) parameter set 2, and (d) fixed width. For completeness also, the pressure distribution associated with a quasi-1D Poiseuille model outcome as well as inviscid fluid are indicated. The geometry is indicated in gray shade and the streamwise direction is normalized x_N. The legend denotes assessed configurations from high to low P/P_0 within the constriction.

accordance with the findings outlined in Sec. 4.1, the influence of the cross-section shape on the model outcome is less pronounced using parameter set 1 than using parameter set 2 or fixed width. Pressure distributions obtained for all cross-section shapes using parameter set 1 approximate the distribution of an ideal fluid for which $\Delta P_{\text{visc}} = 0$ so that the quasi-1D Poiseuille approximation results in a severe underestimation of the pressure drop along the constricted portion. On the other hand, it is seen that for parameter set 2 and fixed width, the magnitude of the pressure drop varies significantly so that, depending on the cross-section shape, the quasi-1D approximation results in an overestimation, an underestimation or an accurate estimation of the pressure drop within the constriction. Note that a rectangular cross-section yields the smallest pressure drop using parameter set 2 and an annulus using fixed width. Moreover, it is observed that imposing a fixed width results in a match between the quasi-1D Poiseuille approximation and the pressure distribution obtained using a rectangular cross-section.

The influence of flow, fluid and geometrical variables — cross-section shape, constriction geometry, dynamic viscosity, upstream pressure and imposed parameter (A or D) — on the pressure distribution is quantified by considering ζ, defined as the ratio of the slope of the normalized pressure drop within the constriction and the slope obtained assuming a quasi-1D Poiseuille model:

$$\zeta = \frac{|P_{\min} - P(x_2)|}{|P_{\min} - P(x_2)|_{\text{Poiseuille}}}, \tag{11}$$

where $P_{\min}$ denotes the minimum pressure. The value $\zeta = 1$ indicates that the quasi-1D Poiseuille model provides an accurate estimate of viscous effects, $\zeta = 0$ corresponds to an inviscid fluid, $\zeta < 1$ indicates an overestimation of viscous effects and $\zeta > 1$ shows that the quasi-1D Poiseuille model results in an underestimation of viscous effects. Values of ζ using parameter set 1, parameter set 2 and fixed width are illustrated in Fig. 9. Different configurations for constriction ratio R_c (30% or
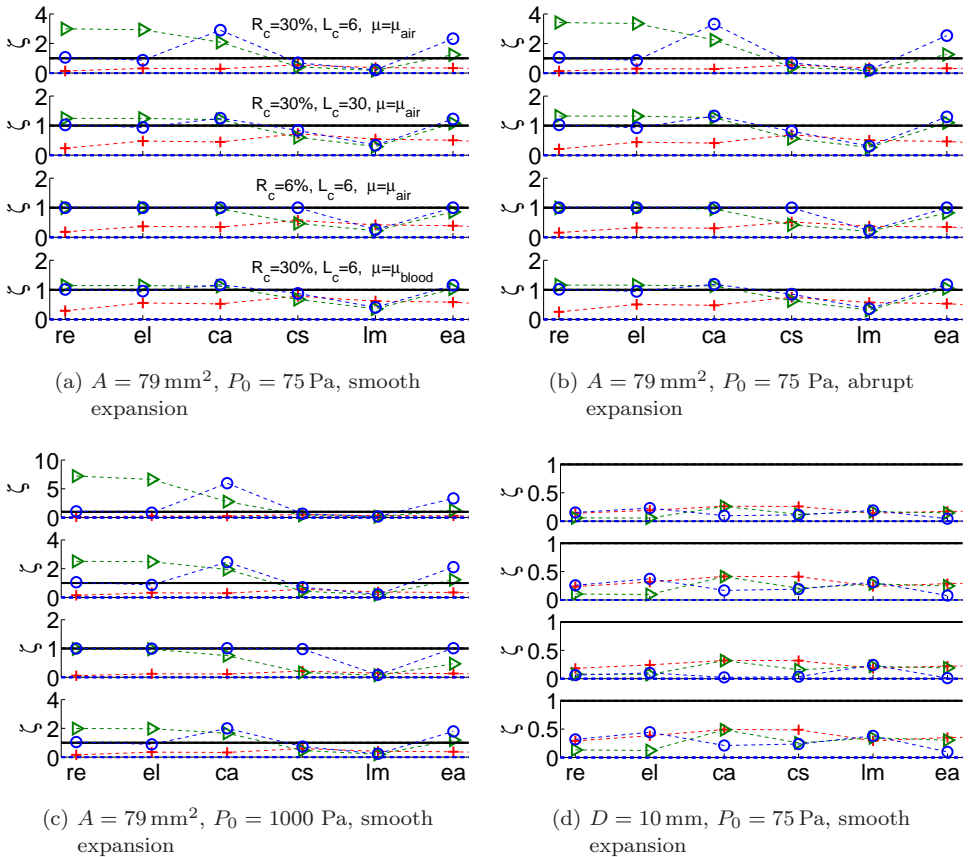

(a) $A = 79\,\text{mm}^2$, $P_0 = 75\,\text{Pa}$, smooth expansion

(b) $A = 79\,\text{mm}^2$, $P_0 = 75\,\text{Pa}$, abrupt expansion

(c) $A = 79\,\text{mm}^2$, $P_0 = 1000\,\text{Pa}$, smooth expansion

(d) $D = 10\,\text{mm}$, $P_0 = 75\,\text{Pa}$, smooth expansion

Fig. 9. Illustration of ζ for parameter set 1 (+), parameter set 2 ($\triangleright$), fixed width ($\circ$) for different geometrical, fluid and flow configurations. For subplots in (b), (d) and (c) values of R_c, L_c and μ are as indicated in Fig. 9(a).

6%), constriction length L_c (6 or 30), dynamic viscosity μ (air or blood), expansion geometry (smooth or abrupt), upstream pressure P_0 (75 Pa or 1000 Pa) and imposed variable (area $A = 79\,\mathrm{mm}^2$ or hydraulic diameter $D = 10\,\mathrm{mm}$) are assessed.

Figure 9(a) shows that when the area A of a smooth expansion is imposed, the quasi-1D Poiseuille model results in either an overestimation (such as parameter set 1) or underestimation (such as parameter set 2) for a rectangular, elliptical and concentric or eccentric annulus cross-section. The magnitude of the over- and, in particular, the underestimation depends on the configuration. In general, it is observed that the underestimation reduces and even disappears for configurations favoring viscous effects such as increasing constriction length L_c ($L_c = 30$), decreasing constriction ratio R_c ($R_c = 6\%$) or yet increasing dynamic viscosity μ ($\mu = \mu_{\mathrm{blood}}$). The overestimation appears to be less sensitive to the exact configuration, including the cross-section shape as observed for parameter set 1. This is also observed using a circular segment or limacon cross-section shape, which is in accordance with previous findings illustrated in Figs. 3 or 8. Imposing the area A of an abrupt instead of a smooth expansion does not alter the observations with respect to the lack of accuracy of the quasi-1D Poiseuille model as illustrated in Fig. 9(b).

Increasing upstream pressure P_0 reduces the impact of viscosity on the flow, so that in accordance with the previous findings, applying the quasi-1D Poiseuille model results in an overestimation or a severe underestimation (600%) of the viscous flow effects. This is illustrated in Fig. 9(c). Results shown in Fig. 9(a) confirm that the underestimation with the quasi-1D Poiseuille model reduces as the geometrical or fluid parameters are altered so that the contribution of viscosity to the pressure distribution within the constriction increases. Moreover, it is seen from Figs. 9(a)–9(c) that the quasi-1D Poiseuille model matches the outcome obtained in the case of a rectangular cross-section shape.

When the hydraulic diameter D is imposed, Fig. 9(d) illustrates that the quasi-1D Poiseuille model overestimates viscous effects, for all assessed configurations. Moreover, the variation of the model outcome for different configurations is small compared to the variation obtained when the area A is imposed.

5. Conclusion

The present paper firstly considers analytical solutions for volume flow rate, velocity distribution and wall shear stress of purely viscous flow through uniform channels with different cross-section shapes. Next, a simplified flow model is proposed for flow through constricted channels which accounts for flow inertia, viscosity as well as cross-section shape. The model outcome is quantified and compared with respect to a quasi-1D model approach accounting for flow inertia and viscosity, which is commonly used to model physiological flow phenomena. The quasi-1D model approach is shown to be inaccurate and the inaccuracy increases for flow and geometrical configurations which are not completely dominated by viscosity. Consequently, present results suggest that when physiological applications are aimed, accounting for the

cross-section shape improves the model accuracy. Shown results for a limited number of cross-section shapes can be used as particular cases to validate numerical solutions for an arbitrary cross-section shape.

Acknowledgments

Appendix

A. Cross-Sections Shapes: Geometrical Parameters

Expressions for area A, hydraulic diameter D and total width y_{tot} for the cross-section shapes depicted in Fig. 1 are given in Table A.1.

Table A.1.   Area A, hydraulic diameter D and total width y_{tot} for cross-section shapes shown in Fig. 1 [Blevins, 1992].

Shape	A	D	y_{tot}
Circle	πa^2	a	$2a$
Ellipse[a]	πab	$\dfrac{4ab}{(a+b)\left(1+\dfrac{h}{4}+\dfrac{h^2}{64}+\dfrac{h^3}{256}\right)}$	$2a$
Rectangle	$4ab$	$\dfrac{4ab}{a+b}$	$2a$
Equilateral triangle	$\dfrac{\sqrt{3}}{4}a^2$	$\dfrac{\sqrt{3}}{3}a$	$\dfrac{\sqrt{3}}{2}a$
Circular segment	$\dfrac{a^2}{2}b$	$\dfrac{2ab}{2+b}$	a
Eccentric annulus	$\pi(a^2-b^2)$	$2(a-b)$	$2a$
Concentric annulus			
Half-moon[b]	$a^2\left(\pi-\theta_2+\dfrac{1}{2}\sin(2\theta_2)\right)$ $-\dfrac{b^2}{2}(\pi-\theta_2-\sin\theta_2)$	$\dfrac{4A}{(\pi-\theta_2)(2a+b)}$	$a+a\cos(\theta_2)$
Limacon	$\pi a^2\left(1+\dfrac{b^2}{2}\right)$	$4a\dfrac{b^2+2}{b^2+4}$	$a(1+b)+\left(\dfrac{1}{4b^2}-\dfrac{a}{2b}\right)$

[a]$h=\dfrac{(a-b)^2}{(a+b)^2}$.
[b]$\theta_2=2\arcsin(\dfrac{b}{2a})$.

Table A.2. $\beta_u(a, b)$ of Eq. (5) for velocity distribution u [Papanastasiou *et al.*, 2000; White, 1991; Piercy *et al.*, 1933; Macdonald, 1893; Berker, 1963].

Shape	$\beta_u(a, b)$
Circle	$\frac{1}{4}(a^2 - r^2)$
Ellipse	$\frac{1}{2}\frac{a^2 b^2}{a^2 + b^2}\left(1 - \frac{y^2}{a^2} - \frac{z^2}{b^2}\right)$
Rectangle[a]	$\frac{1}{2}\left[b^2 - z^2 - \frac{32b^2}{\pi^3}\sum_{n=1,3,\ldots}^{\infty}(-1)^{\frac{n-1}{2}}\frac{\cosh\left(\frac{n\pi y}{2b}\right)\cos\left(\frac{n\pi z}{2b}\right)}{\cosh\left(\frac{n\pi a}{2b}\right)\,n^3}\right]$
Equilateral triangle	$\frac{1}{4\sqrt{3}}\frac{1}{a}(3y^2 - z^2)(2z - \sqrt{3}a)$
Circular segment[a]	$-\frac{1}{4}\left[r^2\left(1 - \frac{\cos 2\theta}{\cos b}\right)\right.$
	$\left.-\frac{16a^2 b^2}{\pi^3}\sum_{n=1,3\ldots}^{\infty}(-1)^{\frac{n+1}{2}}\left(\frac{r}{a}\right)^{\frac{n\pi}{b}}\frac{\cos\left(n\pi\theta/b\right)}{n(n + 2b/\pi)(n - 2b/\pi)}\right]$
Eccentric annulus[a,b,c]	$M^2\left[\sum_{n=1}^{\infty}(-1)^n\frac{e^{-n\beta}\coth\beta\sinh\left(n(\eta - \gamma)\right) - e^{-n\gamma}\coth\gamma\sinh\left(n(\eta - \beta)\right)}{\sinh\left(n(\beta - \gamma)\right)}\right.$
	$\cdot\cos\left(n\xi\right) + \frac{\coth\gamma - \coth\beta}{2(\gamma - \beta)}\eta + \frac{\beta(1 - 2\coth\gamma) - \gamma(1 - 2\coth\beta)}{4(\gamma - \beta)}$
	$\left.-\frac{\cosh\eta - \cos\xi}{4(\cosh\eta + \cos\xi)}\right]$
	$0 < c \leq a - b, \ F = \frac{a^2 - b^2 + c^2}{2c}, \ M = \sqrt{F^2 - a^2}$
	$\gamma = \frac{1}{2}\ln\frac{F + M}{F - M}, \ \beta = \frac{1}{2}\ln\frac{F - c + M}{F - c - M}$
Concentric annulus	$\frac{1}{4}\left[a^2 - r^2 + (a^2 - b^2)\frac{\ln(a/r)}{\ln(b/a)}\right]$
Half-moon	$\frac{1}{4}\left(r^2 - b^2\right)\left(\frac{2a\cos\theta}{r} - 1\right)$
Limacon[d]	$\frac{a^2}{4}\left[1 + 2b\xi + b^2 - (\xi + b(\xi^2 - \eta^2))^2 - (\eta + 2b\xi\eta)^2\right]$
Poiseuille[e]	$-\frac{1}{2}(y^2 - hy)$

[a]Infinite sum is limited to $n \leq 60$.
[b]c yields the distance between inner and outer circle centers.
[c]The mapping is $y + iz = M\tanh\frac{1}{2}(\xi + i\eta)$ with $0 \leq \xi \leq 2\pi$, $\gamma \leq \eta \leq \beta$.
[d]The mapping is $(y, z) = (a(\xi + b(\xi^2 - \eta^2)), \ a(\eta + 2b\xi\eta))$ on the circle $(\xi^2 + \eta^2) \leq 1$.
[e]Quasi-1D approach: height h, $0 \leq y \leq h$.

B. Pressure Driven Viscous Flow Solutions

An overview of terms $\beta_u(a, b)$ of Eq. (5) describing velocity distributions $u(y, z)$ for different cross-section shapes is given in Table A.2. Table A.3 lists the corresponding term $\beta_t(a, b)$ of Eq. (6) yielding wall shear stress τ.

Table A.3. $\beta_t(a, b)$ of Eq. (6) for wall shear stress τ [Haslam and Zamir, 1998; Berker, 1963].

Shape	$\beta_t(a, b)$
Circle	$\dfrac{a}{2}, (r = a)$
Ellipse	$-\dfrac{a^2 b^2}{a^2 + b^2} \sqrt{\dfrac{y^2}{a^4} + \dfrac{z^2}{b^4}}, \left(\dfrac{y^2}{a^2} + \dfrac{z^2}{b^2} = 1\right)$
Rectangle[a]	$\dfrac{8a}{\pi^2} \displaystyle\sum_{n=1,3,\dots}^{\infty} \dfrac{(-1)^{\frac{n-1}{2}}}{i^2} \left[1 - \dfrac{\cosh\left(\dfrac{n\pi z}{2a}\right)}{\cosh\left(\dfrac{n\pi b}{2a}\right)}\right], (y = \pm a)$
	$\dfrac{8a}{\pi^2} \displaystyle\sum_{i=1,3,\dots}^{\infty} (-1)^{\frac{n-1}{2}} \tanh\left(\dfrac{n\pi b}{2a}\right) \dfrac{\cos\left(\dfrac{n\pi y}{2a}\right)}{n^2}, (z = \pm b)$
Equilateral triangle	$-\dfrac{1}{a} z \left(z - \dfrac{\sqrt{3}}{2} a\right), \left(y = \pm\dfrac{\sqrt{3}}{3} z\right)$
	$\dfrac{\sqrt{3}}{2a}\left(y^2 - \dfrac{a^2}{4}\right), \left(z = \dfrac{\sqrt{3}a}{2}\right)$
Circular segment[a]	$-\left[\dfrac{r^2}{4}(1 + 2\tan\alpha) + \dfrac{4a^2\alpha}{\pi^2}\displaystyle\sum_{n=1,3\dots}^{\infty}\dfrac{\left(\dfrac{r}{a}\right)^{\frac{n\pi}{\alpha}}}{\left(n + \dfrac{2\alpha}{\pi}\right)\left(n - \dfrac{2\alpha}{\pi}\right)}\right], \left(\theta = \pm\dfrac{\alpha}{2}\right)$
	$-\dfrac{a}{2}\left[\left(1 - \dfrac{\cos 2\theta}{\cos\alpha}\right) - \dfrac{8\alpha}{\pi^2}\displaystyle\sum_{n=1,3\dots}^{\infty}(-1)^{\frac{n+1}{2}}\dfrac{\cos(n\pi\theta/\alpha)}{\left(n + \dfrac{2\alpha}{\pi}\right)\left(n - \dfrac{2\alpha}{\pi}\right)}\right], (r = a)$
Eccentric[a,b,c] annulus	$-M^2\left[\displaystyle\sum_{n=1}^{\infty}(-1)^n\dfrac{e^{-n\beta}\coth\beta\cosh(n(\eta - \gamma)) - e^{-n\gamma}\coth\gamma\cosh(n(\eta - \beta))}{\sinh(n(\beta - \gamma))}\right.$
	$\left. \cdot n\cos(n\xi) + \dfrac{\coth\gamma - \coth\beta}{2(\gamma - \beta)} - \dfrac{\sinh\eta\cos\xi}{2(\cosh\eta + \cos\xi)^2}\right], (\eta = \gamma, \beta)$
	$0 < c \le a - b, \ F = \dfrac{a^2 - b^2 + c^2}{2c}, \ M = \sqrt{F^2 - a^2}$
	$\gamma = \dfrac{1}{2}\ln\dfrac{F + M}{F - M}, \ \beta = \dfrac{1}{2}\ln\dfrac{F - c + M}{F - c - M}$
Concentric annulus	$\dfrac{1}{4}\left[2b + \dfrac{a^2 - b^2}{b\ln(b/a)}\right], (r = b)$
	$-\dfrac{1}{4}\left[2a + \dfrac{a^2 - b^2}{a\ln(b/a)}\right], (r = a)$

(*Continued*)

Table A.3. (*Continued*)

Shape	$\beta_t(a, b)$
Half-moon	$\dfrac{1}{4}(4a\cos\theta - 2b), (r = b)$
	$-\dfrac{1}{4}\left(\dfrac{b^2}{2a\cos\theta} - 2a\cos\theta\right), (r = 2a\cos\theta)$
Limacon	$-\dfrac{a^2}{2}(1 + 2b\cos\theta + 2b^2)\cos\theta, (0 \leq \theta \leq 2\pi)$
Poiseuille[d]	$y - \dfrac{h}{2}, (y = 0, h)$

[a]Infinite sum is limited to $n \leq 60$.
[b]c yields the distance between inner and outer circle centers.
[c]The mapping is $y + iz = M\tanh\dfrac{1}{2}(\xi + i\eta)$ with $0 \leq \xi \leq 2\pi$, $\gamma \leq \eta \leq \beta$.
[d]Quasi-1D approach: Height h, $0 \leq y \leq h$.

References

Batchelor, G. K. [2000] *An Introduction to Fluid Dynamics* (Cambridge Mathematical Library, Cambridge).

Blevins, R. D. [1992] *Applied Fluid Dynamics Handbook* (Van Nostrand Reinhold, New York).

Berker, R. [1963] *Intégration des Équations du Mouvement d'un Fluide Visqueux Incompressible* (Springer, New York).

Chouly, F. and Lagrée, P. Y. [2012] "Comparison of computations of asymptotic flow models in a constricted channel," *Applied Mathematical Modelling* **36**, 6061–6071.

Cisonni, J., Van Hirtum, A., Pelorson, X. and Willems, J. [2008] "Theoretical simulation and experimental validation of inverse quasi-one-dimensional steady and unsteady glottal flow models," *Journal Acoustical Society of America* **124**, 535–545.

Cisonni, J., Van Hirtum, A., Luo, X. Y. and Pelorson, X. [2010] "Experimental validation of quasi-one-dimensional and two-dimensional steady glottal flow models," *Medical Biological Engineering and Computing* **48**, 903–910.

Gutmark, E. and Grinstein, F. F. [1999] "Flow control with noncircular jets," *Annual Review of Fluid Mechanics* **31**, 239–272.

Haslam, M. and Zamir, M. [1998] "Pulsatile flow in tubes of elliptic cross-sections," *Annals of Biomedical Engineering* **26**, 780–787.

Lekner, J. [2007] "Viscous flow through pipes of various cross-sections," *European Journal of Physics* **28**, 521–527.

Lorhois, S., Lagrée, P. Y., A., Marc-Vergnes, J. P. and Cassot, F. [2000] "Maximal wall shear stress in arterial stenoses: Application to the internal carotid arteries," *Journal of Biomedical Engineering* **122**, 661–666.

Lucero, J., Van Hirtum, A., Ruty, N., Cisonni, J. and Pelorson, X. [2009] "Validation of theoretical models of phonation threshold pressure with data from a vocal fold mechanical replica," *Journal Acoustical Society of America* **125**, 632–635.

Macdonald, H. M. [1893] "On the torsional strength of a hollow shaft," *Proceedings of the Cambridge Philosophical Society* **8**, 62–68.

Milne-Thomson, L. M. [1996] *Theoretical Hydrodynamics* (Dover Publications).

Papanastasiou, T. C., Georgiou, G. C. and Alexandrou, A. N. [2000] *Viscous Fluid Flow* (CRC Press LLC, New York).

Pedley, T. J. and Luo, X. Y. [1998] "Modelling flow and oscillations in collapsible tubes," *Theoretical and Computational Fluid Dynamics* **10**, 277–294.

Piercy, N. A. V., Hooper, M. S. and Winny, H. F. [1933] "Viscous flow through pipes with cores," *Philosophical Magazine Series* **15**, 647–676.

Shapiro, A. H. [1977] "Steady flow in collapsible tubes," *Journal of Biomechanical Engineering* **99**, 126–147.

Shah, R. K. and London, A. L. [1978] *Laminar Flow Forced Convection in Ducts*: *A Source Book for Compact Heat Exchanger Analytical Data* (Academic Press, New York).

Stewart, H. M., Waters, P. S., S. L. and Jensen, O. E. [2010] "Sloshing and slamming oscillations in collapsible channel flow," *Journal of Fluid Mechanics* **662**, 288–319.

Van Hirtum, A., Cisonni, J. and Pelorson, X. [2009] "On quasi-steady laminar flow separation in the upper airways," *Communications in Numerical Methods in Engineering* **25**, 447–461.

White, F. [1991] *Viscous Fluid Flow* (McGraw-Hill, New York).